INTERNATIONAL JOURNAL FOR NUMERICAL METHODS IN FLUIDS
Int. J. Numer. Meth. Fluids 2003; **43**:129–146 (DOI: 10.1002/fld.599)

Coupled lubrication and Stokes flow finite elements

Matthew S. Stay[1] and Victor. H. Barocas[2,*,†]

[1]*Degree Program for Scientific Computing, University of Minnesota, Minneapolis, U.S.A.*
[2]*Department of Biomedical Engineering, University of Minnesota, Minneapolis, U.S.A.*

SUMMARY

A method is developed for performing a local reduction of the governing physics for fluid problems with domains that contain a combination of narrow and non-narrow regions, and the computational accuracy and performance of the method are measured. In the narrow regions of the domain, where the fluid is assumed to have no inertia and the domain height and curvature are assumed small, lubrication, or Reynolds, theory is used locally to reduce the two-dimensional Navier–Stokes equations to the one-dimensional Reynolds equation while retaining a high degree of accuracy in the overall solution. The Reynolds equation is coupled to the governing momentum and mass equations of the non-narrow region with boundary conditions on the mass and momentum flux. The localized reduction technique, termed 'stitching,' is demonstrated on Stokes flow for various geometries of the hydrodynamic journal bearing—a non-trivial test problem for which a known analytical solution is available. The computational advantage of the coupled Stokes–Reynolds method is illustrated on an industrially applicable fully-flooded deformable-roll coating example. The examples in this paper are limited to two-dimensional Stokes flow, but extension to three-dimensional and Navier–Stokes flow is possible.

KEY WORDS: Reynolds–Stokes theory; thin-films; journal bearing; roll coating

1. INTRODUCTION

Early application of the Navier–Stokes (NS) equations to practical problems was limited since the equations could be solved only through analytical means, and for problems that were not axisymmetric and/or included the non-linear inertial terms, analytical solution was, generally, not just difficult, but impossible. Undeterred, researchers of the late 1800s used either mathematical scaling or experimental observations to simplify the fluid momentum equations. The most well-known assumptions were those posed by Reynolds in the 1880s for liquid flows in an annulus [1]. While studying liquid bearings, Reynolds recognized that

*Correspondence to: V. H. Barocas, Deparment of Biomedical Engineering, University of Minnesota, 7-106 BSBE, 312 Church St. SE, Minneapolis, MN 55455, U.S.A.
† E-mail: baroc001@umn.edu

Contract/grant sponsor: Sandia National Laboratory
Contract/grant sponsor: Minnesota Supercomputing Institute

Received 3 February 2003
Revised 19 May 2003

the fluid films were (1) thin and of small curvature, (2) carried little or no inertia, and (3) had no pressure change across their thickness. In conjunction with a mass balance, i.e. the continuity equation, these assumptions are commonly known as lubrication, or Reynolds, theory and served as the basis of analysis for most thin-film problems well into the last century.

With the advent of the digital computer in the 1950s, research into numerical solution of linear and nonlinear partial differential equations saw a dramatic explosion. Concurrently, the finite element method (FEM) was applied to the governing equations of solid structures, where it demonstrated the ability to solve PDEs on arbitrarily shaped domains. Shortly thereafter, the FEM made its way to the world of fluid mechanics and allowed researchers to extend their studies to complex domains. Over time, the FEM has been used to solve countless fluid problems described by the NS equations of motion. Due to the FEM's robust nature, however, the drive to solve the thin-film, or lubrication, equations has been mainly left as a first approximation to the system dynamics. Thus, a dichotomy has arisen for fluid problems that contain a domain with thin-film segments—one uses lubrication theory as a first, sometimes crude approximation or resorts to a FEM solution of the full NS equations. Little effort has been extended to take advantage of lubricated regions within a domain and use Reynolds theory in conjunction with the FEM solution of the NS momentum equations.

The significance of a coupled narrow and non-narrow domain is often lost since computational resources are so abundant that one need not employ the thin-film approximation; one can just go directly to the numerical solution of the NS equations. There is, however, a growing and important class of problems where the thin film region presents a problem for the FEM solution. Difficulty arises in moving boundary problems where a small fraction of the overall domain is lubricated, but the lubricated region of the domain contains information critical to the system dynamics; examples include industrial manufacturing processes like roll coating [2, 3], biotransport in the human eye [4], and the mechanics of cardiovascular valves [5]. Finite element codes that tackle these problems must overmesh the thin region to determine the flow field characteristics and track changes in the domain shape. The shape-tracking problem arises frequently in coupled fluid-solid systems. Although not as common, thin-film regions can also present difficulties when the domain must be modeled with three-dimensional NS and a large fraction of the domain is highly lubricated, as happens with microfluidic channels, pumps, and reactors. Here, the majority of computational resources are devoted to solving a very simple flow field.

While little work in the fluids community has been to done to couple lubrication and NS theory, there has been a large amount of analogous work in the solid and heat transfer communities. Most work to date has focused on the development of models that approximate the displacement or temperature fields by a simple functional form (e.g. a polynomial) with respect to a solid structure's thickness. The complexity of the function is increased until an optimized solution between the dimensionally reduced and the full three-dimensional models is obtained [6, 7]. This approach parallels the development of thin structure theories, determining when and what kind of thin-structure approximation is necessary and giving a measure of the error introduced by the dimensional reduction. Work more directly analogous to the content in this paper is found in References [8–10], where coupling between a thin solid structure, such as a beam or plate, is made with the two- or three-dimensional elasticity equations. The most relevant work on fluids was performed on falling liquid films [11]. The falling film was divided into several zones of flow, the first of which was a NS zone and the last was a

fully developed zone near the bottom of the film. Errors between the NS equations and the fully- developed film were very small.

In this paper, we develop a method for coupling between the thin film lubrication equation and the Stokes equations. We begin by deriving the Reynolds equation in one dimension along an arbitrary curve and show how it can be coupled naturally to the Stokes equations in a finite element formulation. To obtain the error associated with the lubrication approximation, we test the coupling or 'stitching,' on the hydrodynamic journal bearing, which has a known analytical solution for Stokes flow. Finally, we insert the lubrication stitch into the fluid-side dynamics of a model for fully flooded roll coating to demonstrate the future potential of the lubrication approximation in coupled fluid-solid physics problems.

2. GOVERNING EQUATIONS AND FORMULATION

We seek to couple a two- or three-dimensional fluid region, whose physics are governed by the incompressible Stokes momentum and mass conservation equations, to a narrow one- or two-dimensional region, whose physics can be approximated with lubrication, or Reynolds, theory. The following are required to apply lubrication theory: (1) as the fluid enters and travels through the narrow region, its inertia must be negligible, (2) the wall curvature of the narrow region must be small, and (3) the pressure gradient perpendicular to the direction of flow in the narrow region must be negligible. Using the coordinate system depicted in Figure 1, the momentum balance in the thin region simplifies to

$$\frac{\mathrm{d}P}{\mathrm{d}\xi} = \mu \frac{\partial^2 V_\xi}{\partial \eta^2} \tag{1}$$

$$\frac{\partial P}{\partial \eta} = 0 \tag{2}$$

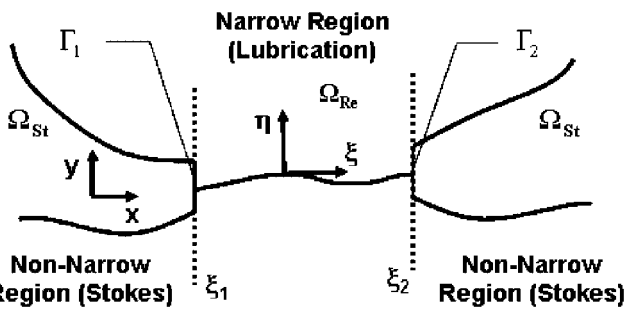

Figure 1. Stokes-lubrication coupling between narrow and non-narrow regions. A two-dimensional, arbitrarily shaped, non-narrow fluid region is connected to a thin narrow region, represented by a one-dimensional arc. The Stokes equations govern the fluid physics in the region Ω_{St}, defined by Cartesian coordinates x and y. A lubrication approximation is made to simplify the governing physics in the thin-film region Ω_{Re}, defined by the coordinates ξ and η which are tangential and normal to the direction of flow, respectively.

where $P(\xi)$ and $V(\xi,\eta)$ are the fluid pressure and velocity in the narrow region. The narrow region coordinates, ξ and η, are tangential and normal to the direction of flow and are used instead of Cartesian coordinates x and y to account for a curved domain. Since we have assumed a small wall curvature, the form of the momentum balance equations is the same as if we had stretched the length of the domain and written the balance with Cartesian coordinates x and y. The narrow region's height is given by a film thickness $h(\xi)$, which can vary over the length of the narrow region. Integrating Equation (1) over the film thickness ($\eta = 0$ to $h(\xi)$) and assigning velocities V_1 and V_2 for the lower and upper boundaries, respectively (both V_1 and V_2 can be functions of ξ, but we have assumed them to be constant for this paper), yields the velocity field for the narrow gap

$$V(\xi,\eta) = \frac{1}{2\mu}\frac{\mathrm{d}P}{\mathrm{d}\xi}(\eta^2 - \eta h) + \frac{1}{2}\left(\frac{V_1 - V_2}{h}\right)\eta + V_1. \tag{3}$$

At this point, we do not know the pressure gradient ($\mathrm{d}P/\mathrm{d}\xi$) along the length of narrow region, but we see clearly that the velocity field is quadratic with respect to η. Integrating across the film thickness again to obtain a flow rate per unit width $Q(\xi)$ we get

$$\begin{aligned} Q &= \int_0^{h(\xi)} \left(\frac{1}{2\mu}\frac{\mathrm{d}P}{\mathrm{d}\xi}(\eta^2 - \eta h) + \frac{1}{2}\left(\frac{V_1 - V_2}{h}\right)\eta + V_1\right)\mathrm{d}\eta \\ &= -\frac{h^3}{12\mu}\frac{\mathrm{d}P}{\mathrm{d}\xi} + \frac{(V_1 + V_2)}{2}h \end{aligned} \tag{4}$$

In order to satisfy the mass balance in the thin region, the flow rate must be constant at every point ξ in the flow path, so we are left with a second order ordinary differential equation in P,

$$\frac{\mathrm{d}Q}{\mathrm{d}\xi} = \frac{\mathrm{d}}{\mathrm{d}\xi}\left(-\frac{h^3}{12\mu}\frac{\mathrm{d}P}{\mathrm{d}\xi} + \frac{(V_1 + V_2)}{2}h\right) = 0 \tag{5}$$

known as the steady-state Reynolds equation, where P is the lubrication pressure.

For the non-narrow region of the fluid domain, the Stokes equations for an incompressible fluid (or the NS equations, as long as assumption (1) from above is true near the transition region) are given by

$$\nabla \cdot \mathbf{T} = 0 \tag{6}$$

$$\nabla \cdot \mathbf{v} = 0 \tag{7}$$

where $\mathbf{T} = -p\mathbf{I} + \mu(\nabla\mathbf{v} + \nabla\mathbf{v}^{\mathrm{T}})$ is the Cauchy stress tensor, p is the pressure, $\mathbf{v}$ is the fluid velocity field, and μ is the fluid viscosity. The boundary of the Stokes domain, $\partial\Omega$, is decomposed into three sections. Sections Γ_1 and Γ_2 represent the two boundaries with the lubrication domain, and section Γ_0 (which need not be connected) represents the remainder of $\partial\Omega$. If we compare Equation (5) and Equations (6), (7), we notice that there is no explicit coupling between the governing equations, so the coupling must be performed at the boundaries. The

goal is to enforce, with minimal error, the mass and momentum balances across the transition interface. Our approach is to set the integrated flow rate out of the Stokes region equal to the lubrication flow rate while specifying the traction on the Stokes surface in terms of the lubrication stress field. Mathematically this is written as

$$\int_{\Gamma_*} \mathbf{n} \cdot \mathbf{v}\, \mathrm{d}S = -Q(\xi_*) \tag{8}$$

$$\mathbf{n} \cdot \mathbf{T}|_{\Gamma_*} = \begin{bmatrix} n_x & n_y \end{bmatrix} \begin{bmatrix} T_{xx} & T_{xy} \\ T_{yx} & T_{yy} \end{bmatrix} = \begin{bmatrix} -n_x P + n_y \dfrac{\mathrm{d}V_\xi}{\mathrm{d}\eta} \\ n_x \dfrac{\mathrm{d}V_\xi}{\mathrm{d}\eta} - n_y P \end{bmatrix}_{\xi_*} \tag{9}$$

where Γ_* and ξ_* ($*=1$ or 2) are the Stokes and lubrication sides, respectively, of the Stokes-lubrication interface defined by Γ in Figure 1. There are, of course, other possible ways of performing the coupling—for example, setting the velocity tangential to the stitch boundary equal to zero and matching normal stresses—but the approach of Equations (8) and (9) is preferred because it can be implemented naturally with the finite element method.

2.1. Galerkin formulation

The majority of incompressible fluids problems that contain a coupling between narrow and non-narrow regions are irregularly shaped, i.e. not logically rectangular or simply mapped, so the Galerkin finite element method (GFEM) is highly attractive. The GFEM has been shown to be highly accurate in solving the NS equations for incompressible liquids and, as will be seen shortly, is particularly suited for implementing the coupling between narrow and non-narrow regions. We recognize that the procedure of forming the finite element weighted residuals for Stokes flow is well known (e.g. Reference [12]), but we present it here to show the coupling between Stokes and lubrication regions. The first step is to multiply the Stokes, continuity, and lubrication equations by separate test functions, $\mathbf{w}^{\mathrm{St}}$, w^{C}, and w^{Re}, and integrate by parts to form the weighted residuals R^{St}, R^{C}, and R^{Re}

$$\begin{aligned} R^{\mathrm{St}} &= \int_\Omega (\nabla \cdot \mathbf{T}) \cdot \mathbf{w}^{\mathrm{St}}\, \mathrm{d}\Omega = 0 \\ &= \int_{\partial\Omega} \mathbf{w}^{\mathrm{St}} \cdot (\mathbf{n} \cdot \mathbf{T})\, \mathrm{d}S - \int_\Omega \nabla \mathbf{w}^{\mathrm{St}} : \mathbf{T}\, \mathrm{d}\Omega \end{aligned} \tag{10}$$

$$R^{\mathrm{C}} = \int_\Omega \nabla \cdot \mathbf{v}\, w^{\mathrm{C}}\, \mathrm{d}\Omega = 0 \tag{11}$$

$$\begin{aligned} R^{\mathrm{Re}} &= \int_{\xi_1}^{\xi_2} \frac{\mathrm{d}Q}{\mathrm{d}\xi} w^{\mathrm{Re}}\, \mathrm{d}\xi = 0 \\ &= Q(\xi_2) w^{\mathrm{Re}}(\xi_2) - Q(\xi_1) w^{\mathrm{Re}}(\xi_1) - \int_{\xi_1}^{\xi_2} Q \frac{\mathrm{d}w^{\mathrm{Re}}}{\mathrm{d}\xi}\, \mathrm{d}\xi \end{aligned} \tag{12}$$

We have replaced ξ_* from Equation (8) with ξ_1 and ξ_2 to indicate the lubrication side of the interface at a thin-film region inlet and outlet. By substituting the relations of Equations (8) and (9) into the boundary terms of the Reynolds and Stokes weighted residuals, respectively, the final residual equations are

$$R^{\mathrm{St}} = -\int_{\Omega} \nabla \mathbf{w}^{\mathrm{St}} : \mathbf{T}\,\mathrm{d}\Omega + \int_{\Gamma_0} \mathbf{w}^{\mathrm{St}} \cdot (\mathbf{n} \cdot \mathbf{T})\,\mathrm{d}S + \int_{\Gamma_1} \left(\left(-n_x P + n_y \frac{\mathrm{d}V_\xi}{\mathrm{d}\eta} \right) w_x^{\mathrm{St}} + \left(n_x \frac{\mathrm{d}V_\xi}{\mathrm{d}\eta} - n_y P \right) w_y^{\mathrm{St}} \right) \mathrm{d}S + \int_{\Gamma_2} \left(\left(-n_x P + n_y \frac{\mathrm{d}V_\xi}{\mathrm{d}\eta} \right) w_x^{\mathrm{St}} + \left(n_x \frac{\mathrm{d}V_\xi}{\mathrm{d}\eta} - n_y P \right) w_y^{\mathrm{St}} \right) \mathrm{d}S \tag{13}$$

$$R^{\mathrm{C}} = \int_{\Gamma_0} \nabla \cdot \mathbf{v}\, w^{\mathrm{C}}\,\mathrm{d}\Omega \tag{14}$$

$$R^{\mathrm{Re}} = -\int_{\Gamma_2} \mathbf{n} \cdot \mathbf{v}\, w^{\mathrm{Re}}(\xi_2)\,\mathrm{d}S + \int_{\Gamma_1} \mathbf{n} \cdot \mathbf{v}\, w^{\mathrm{Re}}(\xi)\,\mathrm{d}S + \int_{\xi_1}^{\xi_2} \left(-\frac{h^3}{12\mu} \frac{\mathrm{d}P}{\mathrm{d}\xi} + \frac{(V_1 + V_2)}{2} h \right) \frac{\mathrm{d}w^{Re}}{\mathrm{d}\xi}\,\mathrm{d}\xi \tag{15}$$

where the integral over Γ_0 is handled by standard techniques based on the boundary conditions. A pictorial example of the coupling between Stokes and lubrication regions is shown in Figure 2. A three-node one-dimensional quadratic element interpolates the lubrication pressure,

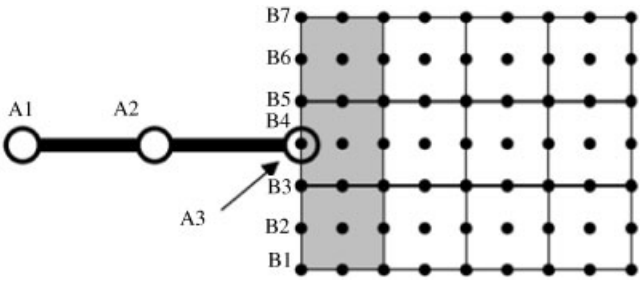

Figure 2. The coupled Stokes–Reynolds transition element. In the finite element discretization, a change from narrow to non-narrow regions is performed with a transition element that connects the one-dimensional lubrication (left) and two-dimensional Stokes finite elements (right). In this example, the Reynolds residual at node A_3, on the single quadratic finite element, is coupled to the residuals along the Stokes boundary, at nodes B_1–B_7. Boundary conditions to the lubrication side of the coupling are supplied by integrating the Stokes velocity field over the boundary of the grey elements to determine the net flow rate out of, or into, the Stokes region. The result is used as the inlet, or outlet, flow rate to the lubrication region. A boundary condition on the Stokes traction, applied to the boundary of the grey elements, is determined from the lubrication stress calculated from the pressure at nodes at A_1–A_3 (see Equations (8) and (9)).

and a nine-node two-dimensional biquadratic element interpolates the Stokes velocity field. The residual equation associated with node A_3 on the lubrication side receives contributions from integrating the Stokes velocity field over the boundary of the gray elements (nodes B_1–B_7). Conversely, the Stokes residuals associated with nodes B_1–B_7 receive contributions from the calculated lubrication stress, which is dependent on the lubrication pressure at node A_1 and the lubrication velocity over element A. Since the lubrication velocity is defined by the lubrication pressure gradient in Equation (3), pressures at nodes A_1–A_3 contribute to the coupling. The coupling strategy is analogous to the solid transition element found in Reference [8]. The fact that fluid mass flows through the Stoke-lubrication element, however, means that the liquid 'transition' element couples an entire side of the Stokes domain to the thin-film region as opposed to a single finite element. That is, if Figure 2 were for a solid instead of a fluid system, only nodes B_3–B_5 would interact with the reduced-dimension element.

2.2. Examples

2.2.1. Large-gap journal bearing. As mentioned in the introduction, dimensionally reducing a region of the Stokes domain to a lubricated approximation results in some error from the full Stokes calculation. The benefit, of course, is that the problem is easier to solve and can be done with smaller computational resources (or with greater accuracy given the same computational resources). In order to assess the error introduced by inserting the lubrication stitch, a non-trivial test problem is needed. To this end, we apply the lubrication stitch to the hydrodynamic journal bearing.

A journal bearing system consists of a stationary outer bearing (physically, a load supporting axle) and an inner rotating journal (a moving axle), which enclose a lubricating fluid—for our purposes, an incompressible liquid. In practical applications, the gap between the journal and bearing is small throughout the entire domain, and the entire fluid domain can be treated with lubrication theory. To demonstrate Stokes–Reynolds coupling, however, we will not restrict ourselves to small gaps. Figure 3(a) depicts the journal bearing and its subdomains, with a lubrication stitch inserted from $\theta = \theta_1$ to $\theta = \theta_2$.

By letting $\xi = R_B\theta$, $V_1 = 0$, and $V_2 = \Omega_J R_J$ we transform the general lubrication equation (5) to

$$\frac{1}{R_B}\frac{d}{d\theta}\left(-\frac{h^3}{12\mu R_B}\frac{dP}{d\theta} + \frac{1}{2}\Omega_J R_J h\right) = 0 \tag{16}$$

where the reference surface for determining the gap is the bearing surface, R_B and R_J are the bearing and journal radii, and Ω_J is the rotational speed of the journal. The bearing is assumed to be stationary for all cases. The resulting Reynolds region finite element residual is

$$R^{Re} = \int_{\theta_1}^{\theta_2}\left(-\frac{h^3}{12\mu R_B}\frac{dP}{d\theta} + \frac{\Omega_J R_J}{2}h\right)d\theta$$

$$-\frac{1}{R_B}\int_{\Gamma_2}\mathbf{n}\cdot\mathbf{v}\,w^{Re}(\theta_2)\,dS + \frac{1}{R_B}\int_{\Gamma_1}\mathbf{n}\cdot\mathbf{v}\,w^{Re}(\theta_1)\,dS \tag{17}$$

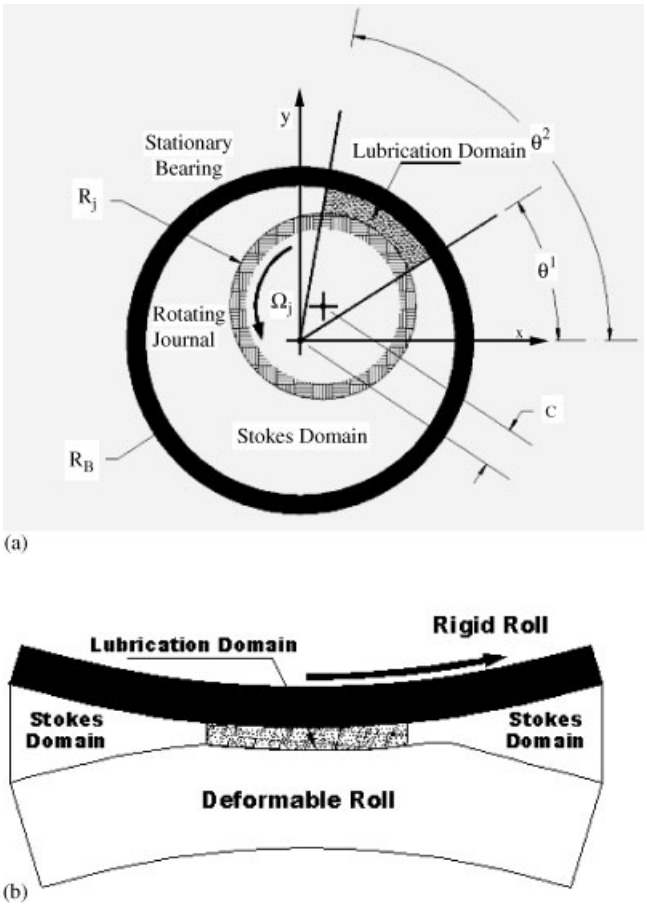

Figure 3. Test problems for Stokes-lubrication coupling: (a) the journal bearing is used to quantify the error associated with introducing the lubrication approximation. The fluid domain is broken into two sections—one where the incompressible Stokes equations (6) and (7) are valid and a second, defined along the arc length from θ_1 to θ_2 where the lubrication equation (5) governs. In (b), the lubrication approximation is introduced into the fully-flooded deformable-roll coating problem (upper rigid roll moving, lower deformable roll stationary). The example demonstrates the computational speed-ups that can be achieved with the coupled Stokes–Reynolds method.

The Stokes equations are unchanged, but the Stokes finite element residual with an appropriately transformed boundary integral is

$$R^{\mathrm{St}} = \int_{\Omega} \nabla \mathbf{w}^{\mathrm{St}} : (-P\mathbf{I} + \mu(\nabla \mathbf{v} + \nabla \mathbf{v}^{\mathrm{T}}))\,\mathrm{d}\Omega + \int_{\Gamma_0} w^{\mathrm{St}}(\mathbf{n} \cdot \mathbf{T})\,\mathrm{d}S$$
$$+ \int_{\Gamma_1} \left(\left(-n_x P(\theta_2) + n_y \frac{\mathrm{d}V_\theta}{\mathrm{d}r} \right) w_x^{\mathrm{St}} + \left(n_x \frac{\mathrm{d}V_\theta}{\mathrm{d}r} - n_y P(\theta_1) \right) w_y^{\mathrm{St}} \right) \mathrm{d}S$$
$$+ \int_{\Gamma_2} \left(\left(-n_x P(\theta_2) + n_y \frac{\mathrm{d}V_\theta}{\mathrm{d}r} \right) w_x^{\mathrm{St}} + \left(n_x \frac{\mathrm{d}V_\theta}{\mathrm{d}r} - n_y P(\theta_1) \right) w_y^{\mathrm{St}} \right) \mathrm{d}S \qquad (18)$$

For the journal bearing, we varied the offset C between the journal and the bearing centers, leading to two different minimum gap thicknesses. The large-gap journal domain was produced by setting minimum gap thickness to 0.025 cm and the small-gap journal was made with a minimum gap of 0.005 cm. In both cases, we varied the length of the stitch. For all of the journal bearing computational experiments, we use a fluid viscosity of $\mu = 1.0$ Poise, a journal radius of $R_J = 0.25$ cm, a bearing radius of $R_B = 0.50$ cm, and a surface velocity on the journal of $V_J = \Omega_J R_J = 1.0$ cm/s. The fluid density is set to zero, eliminating the inertial terms of the NS equations. The Stokes flow problem has a known analytical solution [13].

2.2.2. Roll coater. As a more industrially relevant study, we also solve a fluid–solid problem based on fully flooded deformable-roll coating. A description of the deformable-roll coating process and its uses can be found in Reference [2], along with the governing equations and a procedure for solving the coupled fluid–solid problem. The key features of the model problem are shown in Figure 3(b). The nip region–the narrow gap between the two rolls in near contact—presents a significant computational challenge. A thin liquid film forms, bounded by the counter-clockwise moving rigid upper roll and the stationary but deformable bottom roll. This film is lubricated, but the regions just outside it, on either side, are not. By modeling the nip region as fully flooded (i.e. completely immersed in a liquid) it is reasoned that the nature of the flow in more complex situations, such as free surfaces that form during film splits, can be better understood. As one can imagine, the problem becomes difficult to solve when the liquid film becomes so narrow that a moving mesh used to track the liquid domain becomes distorted and the finite element codes fails. This breakdown could be avoided if a lubrication stitch were inserted in the narrow-gap region when the rolls become close.

To demonstrate the potential of the stitch we used the proprietary code GOMA [14] to solve the fully coupled problem by moving the rigid roll toward the deformable roll. With each successive run of the code, we stepped the rigid roll closer to the deformable roll, using the previous run as an initial guess. GOMA was run until the finite element mesh became so severely distorted that it could not be stepped any closer to the deformable roll no matter what the initial guess. At that point, we saved the configuration of the domain and re-meshed the liquid side with a lubrication stitch included. In similar fashion to the journal bearing, we let $\xi = R_{RR}\theta$, $V_1 = \Omega_{RR} R_{RR}$, and $V_2 = 0$ and transformed the general lubrication equation to

$$R^{Re} = -\frac{1}{R_{RR}} \int_{\Gamma_2} \mathbf{n} \cdot \mathbf{v}\, w^{Re}(\theta_2)\, dS + \frac{1}{R_{RR}} \int_{\Gamma_1} \mathbf{n} \cdot \mathbf{v}\, w^{Re}(\theta_1)\, dS + \int_{\theta_1}^{\theta_2} \left(-\frac{h^3}{12\mu R_{RR}} \frac{dP}{d\theta} + \frac{\Omega_{RR} R_{RR}}{2} h \right) d\theta \tag{19}$$

where R_{RR} and Ω_{RR} are the radius and angular speed of the rigid roll. The Stokes finite element residual becomes

$$R^{St} = \int_{\Gamma_0} \mathbf{w}^{St} \cdot (\mathbf{n} \cdot \mathbf{T})\, dS + \int_{\Omega} \nabla \mathbf{w}^{St} : (-P\mathbf{I} + \mu(\nabla \mathbf{v} + \nabla \mathbf{v}^T))\, d\Omega$$

$$+\int_{\Gamma_1}\left(\left(-n_xP(\theta_2)+n_y\frac{\mathrm{d}V_\theta}{\mathrm{d}r}\right)w_x^{\mathrm{St}}+\left(n_x\frac{\mathrm{d}V_\theta}{\mathrm{d}r}-n_yP(\theta_1)\right)w_y^{\mathrm{St}}\right)\mathrm{d}S$$

$$+\int_{\Gamma_2}\left(\left(-n_xP(\theta_2)+n_y\frac{\mathrm{d}V_\theta}{\mathrm{d}r}\right)w_x^{\mathrm{St}}+\left(n_x\frac{\mathrm{d}V_\theta}{\mathrm{d}r}-n_yP(\theta_1)\right)w_y^{\mathrm{St}}\right)\mathrm{d}S. \qquad (20)$$

3. NUMERICAL EXAMPLES

3.1. *Journal bearing: large gap* ($C = 0.225$ cm)

In Figures 4 and 5 we have plotted the pressure contours and fluid streamtraces of the Stokes segment of the coupled domain. The pressure contours and streamtraces show the general features of the flow field—a large recirculation on the wide-gap side whose arms creep toward the midline of the Stokes domain and a pressure field that is antisymmetric with respect to the same midline. To ascertain the more subtle differences between the full-Stokes and coupled solutions we must probe what happens at the transition between the Stokes and lubrication zones and the lubrication zone itself.

In the thin-film region, defined as θ_1 to θ_2, we have plotted the stitch pressure from the solution of Equation (5) and compared it to the full-Stokes results for the journal and bearing walls. The thin-film pressure plots show that the journal and bearing wall pressures are nearly identical for the entire length of the lubrication domains, even in the long stitch case. As expected, the lubrication pressure, while still a fairly close match for both the short ($\theta_2 - \theta_1 = 5°$) and long ($\theta_2 - \theta_1 = 20°$) stitch cases, becomes worse for a longer stitch. As the lubrication domain gets larger, the interface between the Stokes and Reynolds regions moves closer to the arms of the recirculation zone. Since the radial velocity is obviously non-zero there, the lubrication assumptions break down. As a result, the stitch gets progressively less accurate. By plotting the radial velocity at the Stokes–Reynolds interfaces versus the full-Stokes velocity, we see that the radial velocity and the error between the two solutions is small for the short stitch. For the long stitch, the radial velocity approaches a maximum of 0.15 cm/s which is not trivial compared to the characteristic journal velocity of 1.0 cm/s. This growing radial velocity confirms that the local lubrication approximation is inappropriate.

Although not plotted in the either of the figures, the absolute value of the maximum or minimum pressure serves as a quick method of quantifying the error between the coupled Stokes-lubrication and analytical solutions. For the journal offset of $C = 0.225$cm, the analytical solution peak pressure is 180.363 dyne/cm^2. The coupled short-stitch solution produced a peak pressure of 181.056 dyne/cm^2 (0.4% error) while the coupled long-stitch solution results in a peak pressure of 192.082 dyne/cm^2 (6.5% error), demonstrating that even though the short stitch is much more accurate than the long, both are still fairly successful.

3.2. *Journal bearing: small gap* ($C = 0.245$ cm)

A second way of increasing the degree to which the thin-film region is lubricated occurs by decreasing the gap between journal and bearing. Figures 6 and 7 are analogous to Figures 4 and 5 and show results for a small (1°) and large (4°) lubrication stitch. Stitch lengths were chosen so that the stitch domains would be geometrically similar to those in the large-gap case.

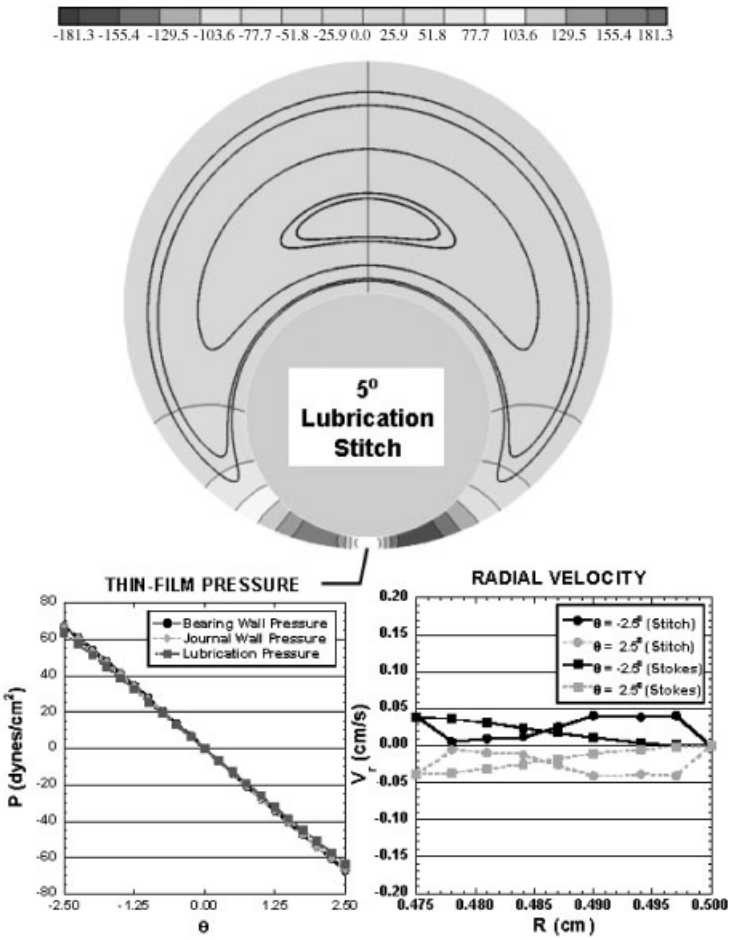

Figure 4. The upper plot shows the pressure contours and streamtraces of the large-gap small-stitch journal bearing system with a lubrication stitch length of 5°. In the lower-left graph, the lubrication pressure is plotted against the journal and bearing wall pressures from the full-Stokes solution. The lower-right graph shows the difference between the coupled model and full-Stokes radial velocities at the Stokes–Reynolds interfaces θ_1 and θ_2. The lubrication approximation assumes that the radial velocity of fluid on the Reynolds side of the Stokes–Reynolds interface is zero, and so the Stokes-side radial velocities serve as a measure of error.

The contour and streamtrace plots suggest that the flow fields compare qualitatively to the analytical solution and, like the solution for the large-gap case, a recirculation forms with an antisymmetric pressure field. The small-gap journal offset is $C = 0.245$ cm, and the analytical solution for the peak pressure is 1874.96 dyne/cm^2. The coupled short-stitch solution produced a peak pressure of 1867.59 dyne/cm^2 (0.4% error), and the coupled long-stitch solution gives a peak pressure of 1902.64 dyne/cm^2 (1.5% error). Unlike the large-gap case, however, the extent to which the arms of the recirculation extend toward the domain midline is much greater, implying that the region over which the stitch is valid will decrease.

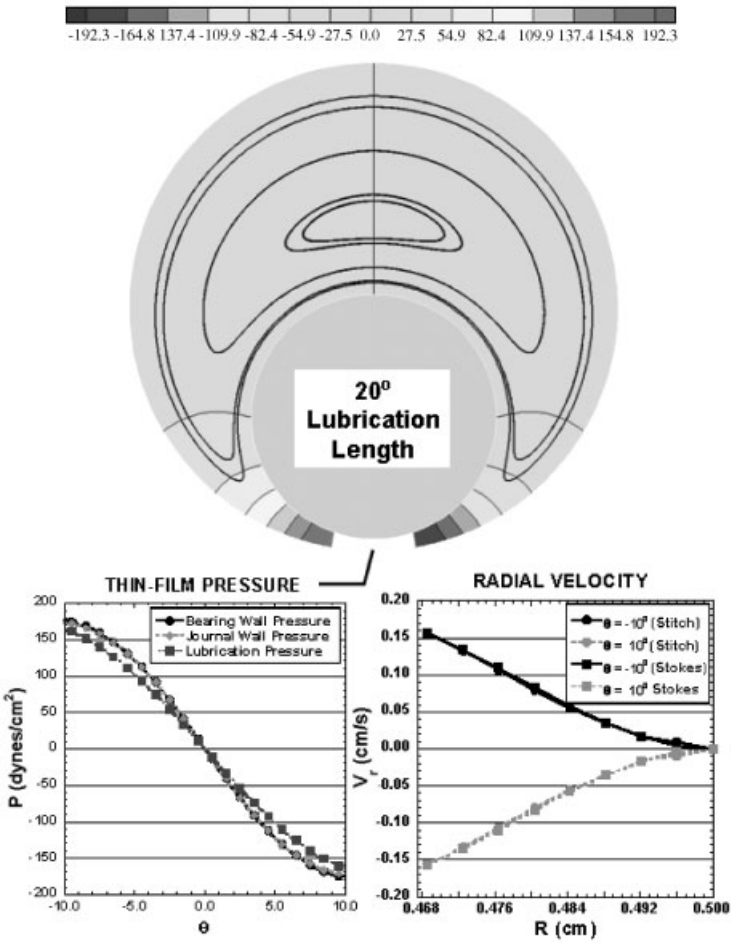

Figure 5. The upper plot shows the pressure contours and streamtraces of the large-gap large-stitch journal bearing system with a lubrication stitch length of 20°. As in Figure 4, we compare the full-Stokes and coupled Reynolds–Stokes narrow region pressures, and plot the radial velocities at θ_1 and θ_2. Even though the radial velocity is approaching a value of 0.15 cm/s, indicating the lubrication approximation is becoming less valid, the difference between the full-Stokes and coupled Stokes-lubrication solution is small.

3.3. Roll coater with the lubrication approximation

Figure 8 shows, in the upper plot, the final domain configuration to the GOMA solution of the fluid-solid problem and, in the lower plot, the pressure field and fluid streamtraces to the full-Stokes solution. The upper rigid roll drags fluid through the narrow portion of the fluid domain and two recirculations form at the inlet and outlet to the nip. The pressure is constant across the thin-film region, which is of small curvature, suggesting that the region is highly lubricated. The results of the coupled Stokes-lubrication model, outlined in Section 2.2.1 and

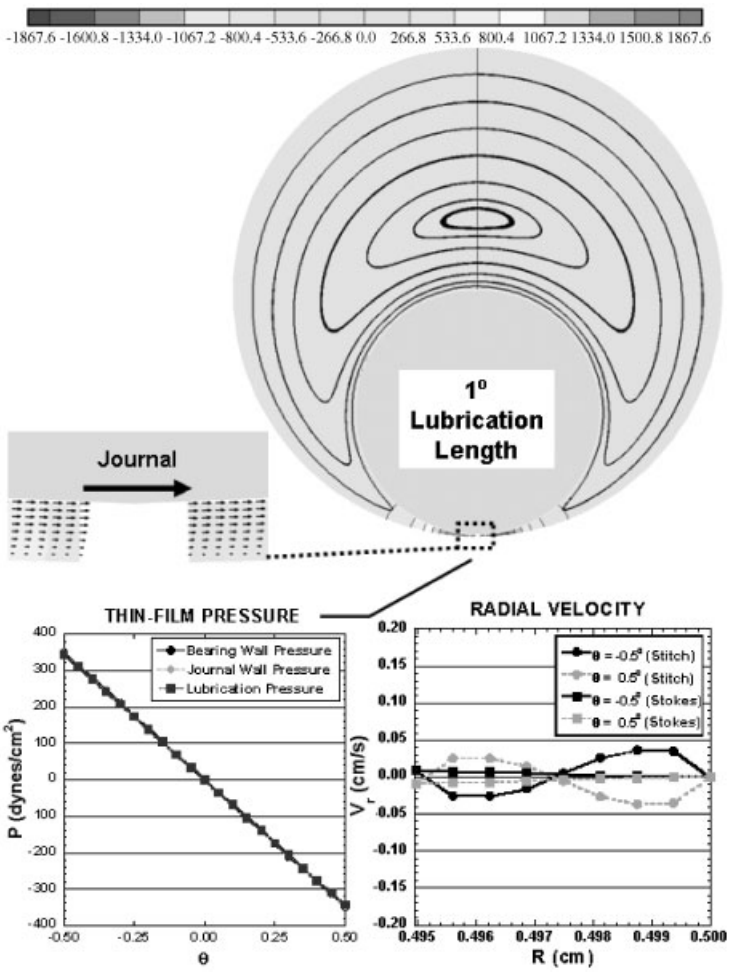

Figure 6. The upper plot includes the pressure contours and streamtraces of the small-gap small-stitch journal bearing system with a lubrication stitch length of 1°. As in Figures 4 and 5 we show the narrow region pressure and Stokes-lubrication interface velocities. A blow-up of the velocity field at the non-narrow to narrow transition is shown in the upper left.

shown in Figure 9, confirm this. A stitch of length 1.4 cm is inserted from $x = -0.7$ cm to $x = +0.7$ cm which removes the troublesome nip section of the domain—the region the mesh would become severely strained in the fully coupled GOMA solution. The pressure contours and streamtraces in Figure 9 closely match those in Figure 8 and the pressure in the lubrication region is virtually indistinguishable from the pressure along the rigid and deformable roll found in the full-Stokes solution. A stitch length greater than 1.5 cm intrudes upon the recirculation zones, where the lubrication approximation breaks down.

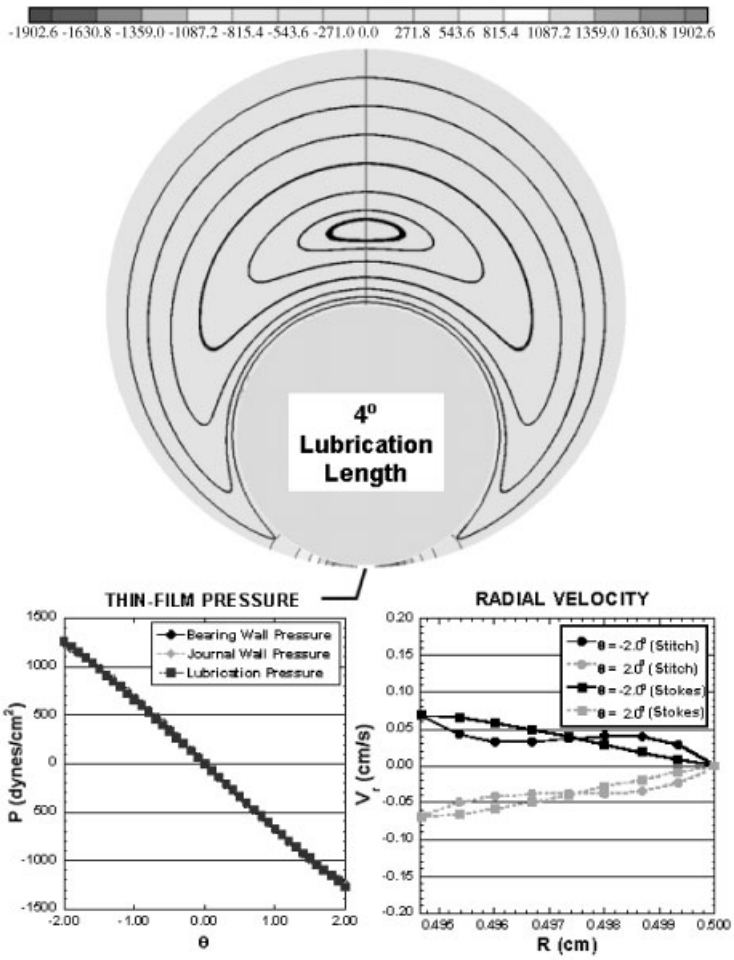

Figure 7. The upper plot includes the pressure contours and streamtraces of the journal bearing system with a lubrication stitch length of 4°.

3.4. Roll coater computational performance

In Figure 10, we have plotted a 'bang-for-the-buck' plot for the roll coating example problem. It shows the CPU time and error between the full-Stokes and stitch models for stitch lengths ranging between 0.1 and 1.4 cm. The difference between the maximum pressure of the Stokes and coupled Stokes-lubrication solutions is used as an error measurement. The maximum pressure of the full-Stokes solution occurs near the centre of the domain and demonstrates that the lubrication region can accurately capture the salient traits of the flow field. Figure 10 shows that for a stitch of length 1.2 cm, a three-fold decrease from the full-Stokes solve-time is achieved, with only 0.2% difference in maximum pressure. The 1.2 cm stitch removed the section of the fluid domain where the large mesh strains would cause the full coupled fluid-solid solver to fail.

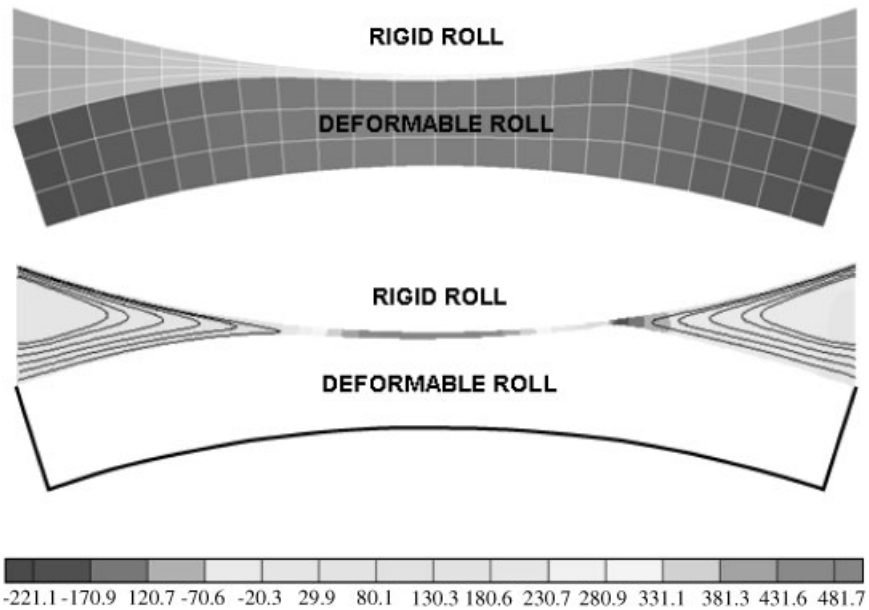

Figure 8. Pressure contours and fluid streamtraces from the solution of the deformable-roll coater problem, before making a local lubrication approximation. The coupled fluid–solid system, described in Reference [2], is solved with GOMA. The plots indicate that the narrow region, between the deformable and rigid rolls, is highly lubricated.

4. DISCUSSION

In both the journal bearing and roll coating examples, we have shown that a local reduction of the governing physics in the narrow region of a coupled narrow/non-narrow domain can be performed with small, but acceptable, error between the coupled and true solutions. For the roll coating problem, a relatively small problem in two dimensions, the lubrication stitch significantly reduced the computational expense—both in memory and CPU time—and a dramatic increase in performance could be achieved in the extension to three dimensions. In both of our examples the non-narrow region is modeled with the Stokes equations, but, an extension to a Navier–Stokes/Reynolds coupling is possible. Since the lubrication theory restrictions are stronger than the Stokes flow restrictions, any region suitable for lubrication theory would necessarily be in the Stokes regime locally.

Solution of our example problems suggests that the implementation of a stitch requires an understanding of the effect of the velocity and pressure fields from the Stokes domain on the apparent Reynolds domain, and the distance of their influence. Suppose, for example, that there is a narrow region that meets the basic requirements for lubrication theory - $(\mathrm{d}h/\mathrm{d}\xi)^2 \ll 1$, $h/R \ll 1$, $Re_\eta \ll 1$—adjacent to a region that does not. Scaling arguments based on the entire length of the Reynolds subdomain, denoted by L, require that the pressure gradient in the η direction be negligibly small, but $\mathrm{d}p/\mathrm{d}\eta$ does not need to be zero at the boundary between the Stokes and Reynolds regions because of the complex flow field allowed on the Stokes side. If $\mathrm{d}p/\mathrm{d}\eta$ is non-zero at the boundary, the pressure gradient will penetrate into the Reynolds

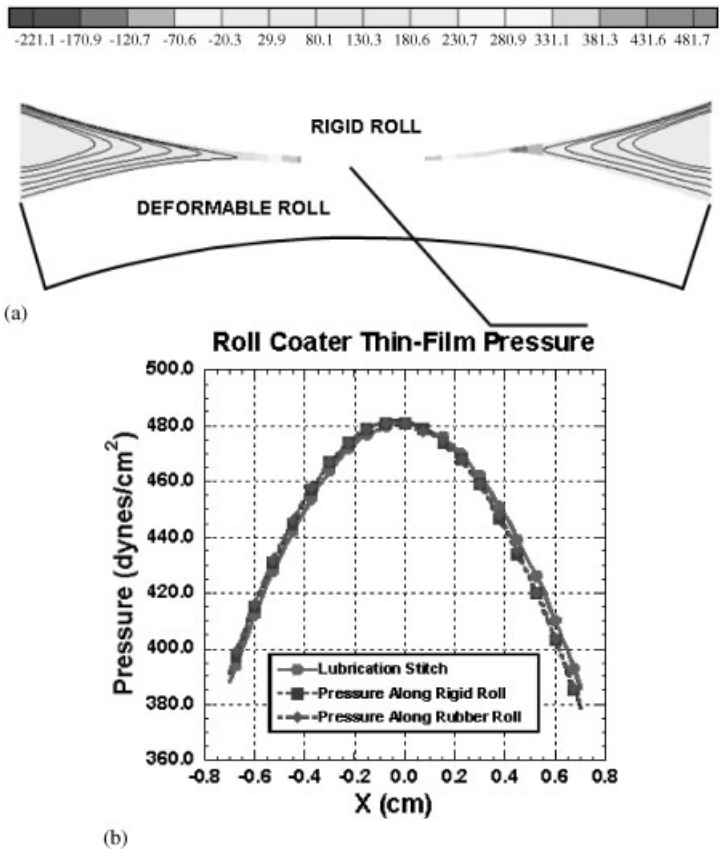

Figure 9. Roll coating pressure and streamtraces with a stitch: (a) an example of the coupled Stokes-lubrication solution to the fluid dynamics of the roll coater—in this example, the lubrication approximation connecting the two Stokes regions has a length of 1.4 cm; and (b) comparison of the lubrication pressure and the rigid and deformable wall pressures. The rigid and deformable wall pressures are taken from the full-Stokes solution shown in the previous figure.

domain some small distance δ, and the stitch must have a buffer to capture the entrance effects. The length of the entrance region can be estimated by applying the same scaling analysis to the Stokes equations as in lubrication theory, except that the ξ length scale is set to δ rather than L. Assigning a characteristic ξ-velocity U, a characteristic η-velocity V, and characteristic pressure P^*, we get the following dimensionless equation:

$$\left(\frac{U\mu}{\delta^2}\right)\frac{\partial^2 v_\xi}{\partial \xi^2} + \left(\frac{U\mu}{h^2}\right)\frac{\partial^2 v_\xi}{\partial \eta^2} - \left(\frac{P^*}{\delta}\right)\frac{\partial p}{\partial \xi} = 0 \tag{21}$$

$$\left(\frac{U\mu}{\delta^2}\right)\frac{\partial^2 v_\eta}{\partial \xi^2} + \left(\frac{U\mu}{h^2}\right)\frac{\partial^2 v_\eta}{\partial \eta^2} - \left(\frac{P^*}{h}\right)\frac{\partial p}{\partial \eta} = 0 \tag{22}$$

$$\left(\frac{U}{\delta}\right)\frac{\partial v_\xi}{\partial \xi} + \left(\frac{V}{h}\right)\frac{\partial v_\eta}{\partial \eta} = 0 \tag{23}$$

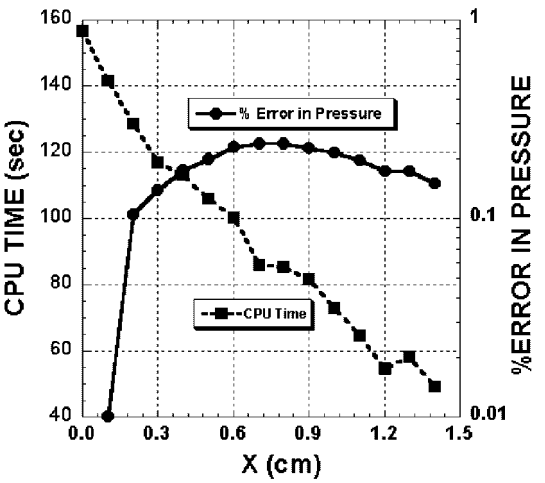

Figure 10. The difference between the peak pressure calculated with GOMA and the peak pressure calculated with the coupled Stokes–Reynolds code is plotted against stitch length. The CPU solve-time is also plotted against stitch length. The roll coating example demonstrates that as the lubrication stitch increases, a substantial decrease in the CPU solve-time can be achieved—with little increase in the solution error.

The continuity equation (23) thus requires that $V \sim Uh/\delta$. Similarly, if we assume for the moment that $\delta \geqslant h$, we can use the last two terms of the ξ momentum equation (21) and conclude that $P^* \sim U\mu\delta/h^2$. Substituting into the η momentum equation (22) gives terms with lead scaling $(U\mu h/\delta^3)$, $(U\mu/\delta h)$, and $(U\mu\delta/h^3)$. Since we are interested in the region where the (last) pressure term does not dominate, we conclude that $\delta \sim h$, which is also internally consistent with our analysis of the ξ momentum equation. We therefore conclude that there must be an $O(h)$ buffer at each end of the stitch to prevent pollution by the Stokes domain solution.

This effect is quite clear in our journal bearing results. The gap thickness h may be shown by simple geometry to be given by $h(\theta) = R_B - C\cos(\theta) - \sqrt{(R_J^2 - C\sin^2(\theta))}$ allowing us to calculate $\mathrm{d}h/\mathrm{d}\xi\,(= 1/R_B\,\mathrm{d}h/\mathrm{d}\theta)$. Suppose, for example, that we wish to limit $\mathrm{d}h/\mathrm{d}\xi$ to 0.1 for the Reynolds region. The limits are then $\theta = \pm 13.6°$ for the large gap and $\theta = \pm 11.9°$ for the small gap. For the large gap, the 20° stitch ($\theta = \pm 10°$) is only about 0.7 gap widths away from the critical value, so it is not surprising that there is significant transverse flow and loss in accuracy. For the small gap, even though the 4° stitch has roughly the same aspect ratio as the 20° stitch does for the large gap, it is much farther from the critical θ value, about 5.4 gap widths away. This result explains why, even though the recirculation extends farther toward the gap in the small-gap case, the effect of it is smaller—the radial velocity for the 4° stitch in the small gap is only about one third to one half of that in the 20° stitch in the large gap.

Finally, our example problems were chosen because they fall into a class of steady-state fluid systems where the existence and location of the lubrication region was known *a priori*, but many, if not most, physically interesting problems are not steady, making it difficult to

know when and where a lubrication stitch is applicable. A simple example of this would occur if we applied a force to the journal boundary and calculated its movement in time. Initially, the journal would sit near the center of the domain and the Stokes equations would be used to determine the characteristics of the flow field. In response to the applied force, the journal would more toward the bearing wall, creating a narrow region between the journal and bearing. If the Reynolds number and curvature ($dh/d\xi$) are much less than 1, a lubrication stitch could be inserted and the coupled Stokes-lubrication model could be solved. The hydrodynamic pressure would then rise and force the journal back to the domain center, provided the journal was not carrying too much inertia. As the local domain curvature and Reynolds number increase, a large mismatch between the stress on the Stokes and lubrication portions of the stitch interface would arise. The coupled Stokes-lubrication model could be turned off and the full-Stokes solution would then be needed again. Therefore, the next generation of stitch development should be dynamic in nature to handle transient fluid physics.

ACKNOWLEDGEMENTS

This work was supported by the U.S. Department of Energy through Sandia National Laboratories (Albuquerque, NM) and by a supercomputing resources allocation grant from the Minnesota Supercomputing Institute. We also specifically acknowledge Sandia's Engineering Sciences Center for granting us the use of GOMA.

REFERENCES

1. Reynolds O. On the theory of lubrication and its application to Mr. Beauchamp tower's experiments, including an experimental determination of the viscosity of olive oil. *Philosophical Transactions of the Royal Society of London* 1886; **177**:157–234.
2. Carvalho MS, Scriven LE. Flows in forward deformable roll coating gaps: comaparison between spring and plane-strain models of roll cover. *Journal of Computational Physics* 1997; **138**:449–479.
3. Roy RV, Roberts AJ, Simpson ME. A lubrication model of coating flows over a curved substrate in space. *Journal of Fluid Mechanics* 2002; **454**(10):235–261.
4. Heys JJ, Barocas VH, Taravella MJ. Modeling passive mechanical interaction between aqueous humor and iris. *Journal of Biomechanical Engineering* 2001; **123**(6):540–547.
5. Lai YG, Chandran KB, Lemmon J. A numerical simulation of mechanical heart valve closure fluid dynamics. *Journal of Biomechanics* 2002; **35**:881–892.
6. Cho JR, Oden JT. A priori modeling error estimates of hierarchical models for elasticity problems for plate- and shell-like structures. *Mathematical and Computer Modelling* 1996; **23**(10):117–133.
7. Ainsworth M, Arnold M. Construction and analysis of optimal hierarchic models of boundary value problems on thin circular and spherical geometries. *SIAM Journal for Scientific Computing* 2000; **22**(2):673–703.
8. Surna KS. Transition finite elements for three-dimensional stress analysis. *International Journal for Numerical Methods in Engineering* 1980; **15**:991–1020.
9. Liao CL, Reddy JN, Engelstad SP. A solid-shell transition element for geometrically non-linear analysis of laminated composite structures. *International Journal for Numerical Methods in Engineering* 1988; **26**:1843–1854.
10. McCune RW, Armstrong CG, Robison DJ. Mixed-dimensional coupling in finite element models. *International Journal for Numerical Methods in Engineering* 2000; **49**:725–750.
11. Kistler SF. The fluid mechanics of curtain coating and related viscous free surface flow with contact lines. *Ph.D. Thesis*, University of Minnesota, 1983.
12. Strang G, Fix GJ. *An Analysis of the Finite Element Method*. Prentice-Hall: Englewood Cliffs, NJ, 1973.
13. Jeffery GB. The rotation of two circular cylinders in a viscous fluid. *Proceedings of the Royal Society of London* 1922; **101**(709):169–174.
14. Schunk PR, Sackinger PA, Rao RR, Chen KS, Baer TA, Labreche DA, Sun AC, Hopkins MM, Subia SR, Moffat HK, Secor RB, Roach RA, Wilkes ED, Noble DR, Hopkins PL, Simmons J, Notz PK. GOMA 4.0—A Full-Newton finite element program for free and moving boundary problems with coupled fluid/solid momentum, energy, mass, and chemical species transport: *user's guide*, Sandia National Laboratories, Albuquerque, 2002.

